EXPERIMENT ON SMRF CONSIDERING MULTIPLE EARTHQUAKES PART 2 TEST RESULTS

K. Kohtaki[1], R. Tenderan [2], T. Isihda[3], S. Yamada[4], S. Kishiki[5],
T. Seike[6], T. Hasegawa[7], J. Iyama[8], S. Yagi[9], N. Tatsumi[10]

[1] *Graduate student, Tokyo Institute of Technology, kotaki.k.aa@m.titech.ac.jp*
[2] *Graduate student, Tokyo Institute of Technology, tenderan.r.aa@m.titech.ac.jp*
[3] *Assistant Prof., Tokyo Institute of Technology, ishida.t.ae@m.titech.ac.jp*
[4] *Prof., Tokyo Institute of Technology, yamada.s.ad@m.titech.ac.jp*
[5] *Associate Prof., Tokyo Institute of Technology, kishiki.s.aa@m.titech.ac.jp*
[6] *Prof., The University of Tokyo, seike@edu.k.u-tokyo.ac.jp*
[7] *Chief Researcher, Building Research Institute, hase@kenken.go.jp*
[8] *Associate Prof., The University of Tokyo, iyama@arch1.t.u-tokyo.ac.jp*
[9] *Graduate student, The University of Tokyo, 6952829840@edu.k.u-tokyo.ac.jp*
[10] *Assistant Prof., Tokyo Institute of Technology, tatsumi.n.aa@m.titech.ac.jp*

Abstract

In this study, a cyclic loading test considering multiple earthquakes was conducted to a full-scale steel moment-resisting frame (SMRFs) specimen. The test specimens and the loading protocol are reported in Part 1. In this part, the test result of both specimens (LGS frame and ALC frame) are reported. In addition, the evaluation of seismic performance under multiple earthquakes will be discussed. As explained in Part 1, the loading protocol used in this experiment consists of multiple sets of loading history in which one set of loading history corresponds to a certain intensity level of earthquake.

From the test result, various comparisons of the performance of specimens are discussed. In terms of the structural performance, it is found that in both specimens, the ductile fracture firstly occurred in the plane frame with the weld access hole beam-to-column connection detail. When the bottom flange of the beam with the weld access hole detail is fully fractured, only a small crack developed in the beam connection without weld access hole detail. Moreover, the performance of the nonstructural components is compared, it is found that the damage that may affect the functionality as a building firstly occurred at the LGS wall, while at the same time, the ALC panel was almost undamaged. It is also found that the openings, either on the LGS wall or ALC panel, influence the damage of the nonstructural components. In addition, the influence of attaching nonstructural components to the shear strength of the frame is also analyzed. The amount of shear force resisted by the nonstructural components is estimated by subtracting the total input shear force with the shear force resisted by the steel frame. In this test, it is found that the nonstructural components are affected the whole shear strength of the frame, especially in the case of the LGS wall, because the LGS wall was attached inside the plane frame. The LGS wall is estimated to resist about 33% of the whole shear force.

Furthermore, the influence of multiple sets of loading on seismic performance was analyzed, not only on the steel frame but also on the nonstructural components. One of the findings is the maximum strength and stiffness of steel frame are barely deteriorated even when a small crack at the toe of weld access hole and a local buckling are generated around the beam-to-column connection; as during the test, the crack and local buckling eventually occurred after multiple sets of loading including three sets which correspond with a deformation during a large earthquake (two sets with maximum story drift angle of 1/75 rad and one set with that of 1/50 rad). Additionally, the influence of multiple sets of loading on various parameters are also analyzed and will be presented in this paper.

Keywords: Steel moment-resisting frame; Cyclic loading test; Multiple earthquakes

1. Introduction

In this study, a cyclic loading test considering multiple earthquakes was conducted to a full-scale steel moment-resisting frame (SMRFs) specimen. In Part 1, the outline of the test including specimens, loading protocol, and measurement plan is explained. In this part, the experimental progress and load-deformation relationship of this test are presented. In addition, the functionality and seismic performance of steel buildings subjected to multiple earthquakes are evaluated.

2. Experimental Progress

In this section, the experimental progress of each specimen is reported, and the functionality of steel building subjected to multiple earthquakes is evaluated.

2.1 Experimental progress of LGS frame

The experimental progress of the LGS frame in each set is shown below.

■ Set No. 1 (R_{max} = 1/400, Level 1)

In nonstructural components, a crack of LGS wall painting was generated around the opening at -1.0 R_{max} (Photo 1). In structural components, no damage was observed.

■ Set No. 2 (R_{max} = 1/200, Level 1)

In nonstructural components, previous crack (Photo 1) reached the gypsum board (Photo 2). In structural components, slab crack due to negative bending was generated at -1.0 R_{max} (Photo 3).

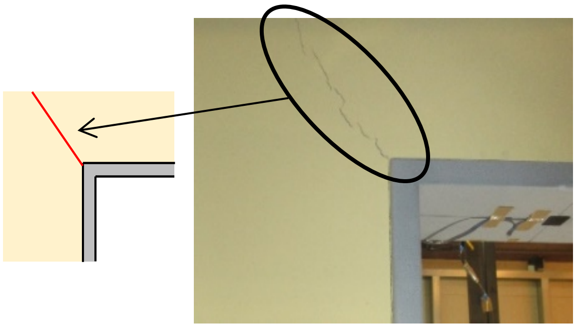

Photo 1 – Crack around the opening of LGS wall

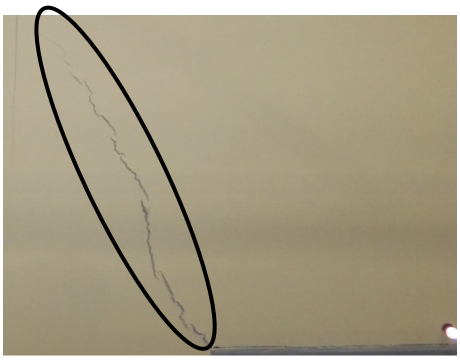

Photo 2 – Crack reaching the gypsum board

Photo 3 – Slab crack due to negative bending

■ Set No. 3 (R_{max} = 1/100, Level 2)

In structural components, the lower beam of the steel frame was yield, and the peeling of the mill scale was observed in the lower flange of the lower beam end.

■ Set No. 4 (R_{max} = 1/200, Level 1)

No new damage was found in structural components and nonstructural components.

■ Set No. 5 (R_{max} = 1/75, Level 3)

In nonstructural components, the foundation frame of the LGS wall around the eccentric part was detached at -1.0 R_{max} (Photo 4). In structural components, slab crack due to positive bending was generated at the first cycle of ±0.6 R_{max} (Photo 5).

■ Set No. 6 (R_{max} = 1/100, Level 2)

No new damage was found in nonstructural components and slab crack was slightly developed in structural components.

■ Set No. 7 (R_{max} = 1/50, Level 3)

In nonstructural components, gypsum boards in the flat part (E-plane) was deformed out-of-plane. In structural components, the crack at the toe of the weld access hole (E-plane) of the lower beam end was generated at the first cycle of +0.8 R_{max} (Photo 6). In addition, local buckling of the lower flange at the lower beam end occurred in both planes at -1.0 R_{max} (Photo 7).

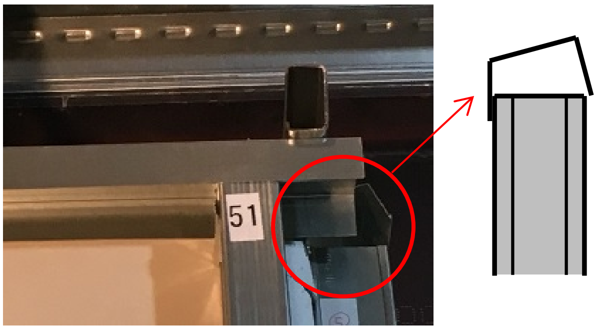

Photo 4 – Detachment of LGS foundation frame

Photo 5 – Slab crack due to positive bending

Photo 6 – Crack at the toe of the weld access hole

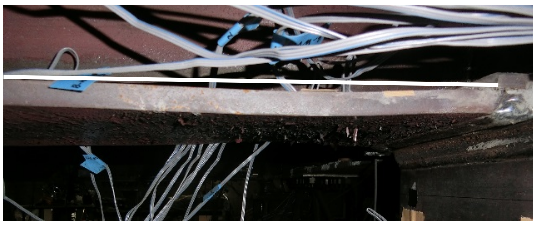

Photo 7 – Local buckling of beam end

■ Set No. 8 (R_{max} = 1/75, Level 3)

No new damage was found in nonstructural components and slab crack was developed in structural components.

■ Set No. 9 (R_{max} = 1/33, Level 4)

In nonstructural components, gypsum boards in flat part (E-plane) were largely deformed out-of-plane and fell off at unloading after -1.0 R_{max} (Photo 8). In structural components, the crack initiated from the toe of the weld access hole (E-plane) at the lower beam end was penetrated at -1.0 R_{max} (Photo 9). In addition, a small crack was generated at the weld toe of the lower flange of the W-plane lower beam.

■ Constant amplitude loading (1/33)

After completing all the nine sets of loading, the test was continued by applying the constant amplitude of R = 1/33 to observe the ultimate behavior of the steel frame. The lower flange of the E-plane lower beam end was fractured at cycle 1- (Photo 10), and the crack at the toe of the weld access hole (E-plane) of the upper beam end was penetrated at the cycle 10-. The loading was stopped at the cycle 11+ because the crack at the web of the E-plane lower beam reached 3/4 of the section height (Photo 11(a)). Photo 11 shows the beam end condition of the LGS frame at the final loading. Almost all sections fractured at the plane with a weld access hole (E-plane); on the contrary, almost no crack was generated at the plane without a weld access hole (W-plane).

Photo 8 – Gypsum board fell off

Photo 9 – Crack penetration at the toe of the weld access hole

Photo 10 – Lower flange fracture at E-plane

(a) E-plane

(b) W-plane

Photo 11 – Beam end condition of LGS frame at the final loading

2.2 Experimental progress of ALC frame

The experimental progress of the ALC frame in each set is shown below.

■ Set No. 2 (R_{max} = 1/200, Level 1)

In nonstructural components, the mortar between slab and ALC panel crack due to negative bending was generated at ±0.4 R_{max} (Photo 12). In structural components, slab crack due to negative bending was generated at the first cycle of -0.8 R_{max} (Photo 13).

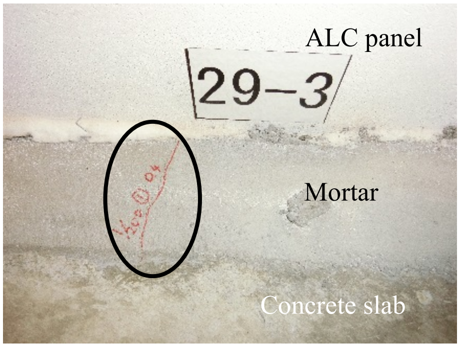

Photo 12 – Crack at the mortar due to negative bending

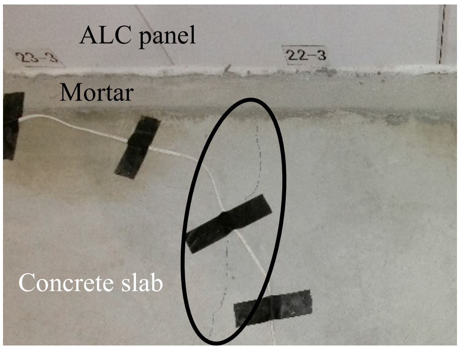

Photo 13 – Crack at the slab due to negative bending

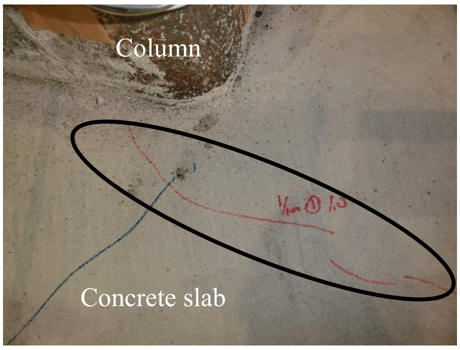

Photo 14 – Crack at the slab due to positive bending

■ Set No. 3 (R_{max} = 1/100, Level 2)

In nonstructural components, previous damage was developed but no new damage was observed. In structural components, slab crack due to positive bending was generated at ±1.0 R_{max} (Photo 14).

■ Set No. 4 (R_{max} = 1/200, Level 1)

No new damage was found in structural components and nonstructural components.

■ Set No. 5 (R_{max} = 1/75, Level 3)

In nonstructural components, previous damage was developed but no new damage was observed. In structural components, local buckling of the lower flange at the lower beam end occurred in both planes at ±1.0 R_{max}.

■ Set No. 6 (R_{max} = 1/100, Level 2)

No new damage was found in nonstructural components and slab crack was slightly developed in structural components.

■ Set No. 7 (R_{max} = 1/50, Level 3)

In nonstructural components, crack at the ALC panel was generated around the opening at the first cycle of -0.8 R_{max} (Photo 13). In structural components, the crack at the toe of the weld access hole (E-plane) of the lower flange at the lower beam end was generated at the first cycle of -0.6 R_{max} (Photo 16).

■ Set No. 8 (R_{max} = 1/75, Level 3)

No new damage was found in nonstructural components and slab crack was developed in structural components.

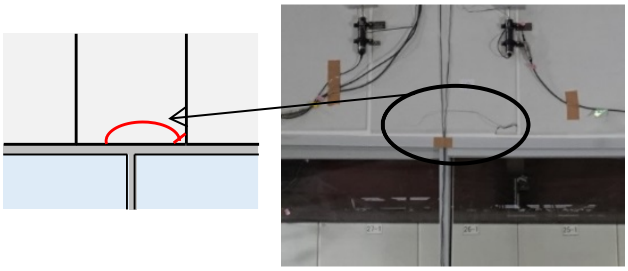

Photo 15 – Crack at the ALC panel around opening

Photo 16 – Crack at the toe of the weld access hole

Photo 17 – Crack penetration at the toe of the weld access hole

■ Set No. 9 (R_{max} = 1/33, Level 4)

In nonstructural components, previous damage was developed but no new damage was observed. In structural components, crack initiated from the toe of the weld access hole (E-plane) of the lower flange was penetrated at the second cycle of -0.6 R_{max} (Photo 17).

■ Constant amplitude loading (1/50)

After completing all the sets of loading, the test was continued by applying the constant amplitude of R = 1/50 to observe the ultimate behavior of the steel frame. The lower flange of the E-plane lower beam end was fractured at cycle 5- (Photo 18); thus, the loading was stopped. In addition, there is almost no damage found in the ALC panel without openings (E-plane) at the end of the loading (Photo 19).

Photo 18 – Lower flange fracture at E-plane

Photo 19 – Final condition of ALC wall in E-plane

In order to evaluate the functionality of steel building subjected to multiple earthquakes, experimental progress of LGS wall and ALC wall are compared. In the LGS frame, the crack of the gypsum board around the opening was generated at Set No. 2 (Level 1), and detachment of the foundation frame was observed at Set No. 5 (Level 3). At the same set, only slab crack was observed in the steel frame. From that comparison, it can be implied that the damage of the LGS wall which might affect the function of the building occurred even when there was almost no damage in the steel frame. In addition, gypsum boards in the flat part (E-plane) fell off at Set No. 9 (Level 4). Meanwhile, at the same set, in the steel frame, crack at the toe of the weld access hole was penetrated but not fully fractured yet, and there was almost no crack at the beam end without a weld access hole. In the ALC frame, the crack of the ALC panel was generated at Set No. 7 (Level 3). At the same set, a small crack at the toe of the weld access hole and small deformation of local buckling at the beam ends were generated in the steel frame. In addition, the ALC wall without opening (E-plane) was almost undamaged even when the lower flange of the steel beam was fractured. Based on that comparison, it could be concluded that the functionality of steel building subjected to multiple earthquakes might be governed by the damage of the LGS wall (interior wall) rather than the ALC wall (exterior wall) and the steel frame.

3. Load-Deformation Relationship

In this section, the load-deformation relationship of each specimen is reported and the seismic performance of steel building subjected to multiple earthquakes is evaluated. Fig. 1 and 2 show the load-deformation relationship of LGS frame in loading sets considering multiple earthquakes and constant amplitude loading, respectively. Meanwhile, Fig. 3 and 4 show those of ALC frame in loading sets and constant amplitude loading, respectively. In Fig. 1 and 3, three types of load-deformation relationship are shown, i.e., whole specimen (structural component + nonstructural component) ((a) in figure), structural component (steel frame) only ((b) in figure), and nonstructural component (LGS wall or ALC wall) only ((c) in figure). The calculation method of each shear force is explained in Part 1. In every graph, the shear force and the percentage resisted by the structural and nonstructural components at the R_{max} of the loading set are also shown.

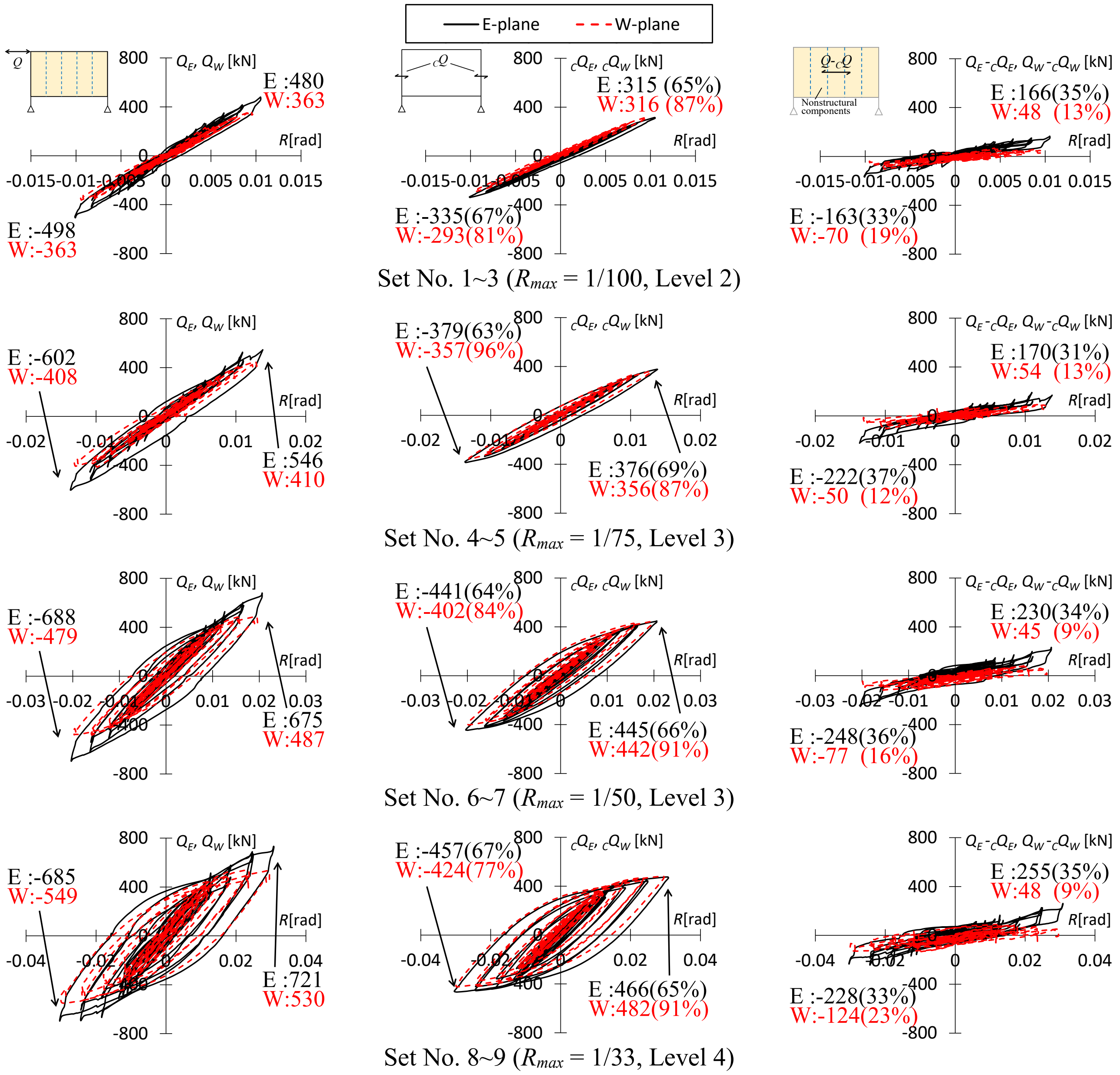

(a) Whole (b) Steel frame (c) Nonstructural components

Fig. 1 – Load-deformation relationship of LGS frame

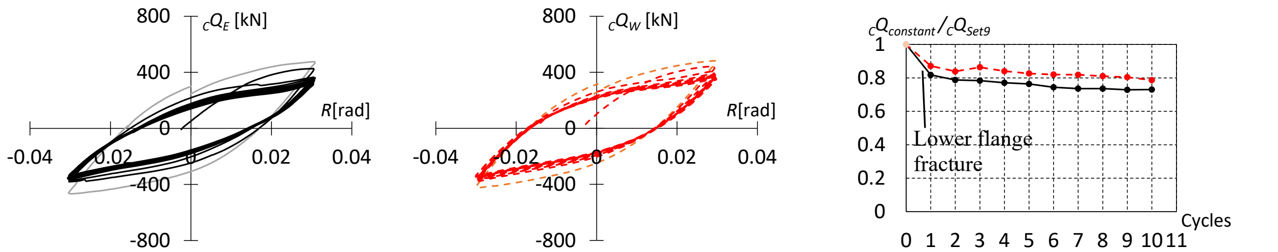

(a) E-plane (b) W-plane (c) Deterioration of maximum strength

Fig. 2 – Load-deformation relationship of the steel frame in constant amplitude loading (1/33) of LGS frame

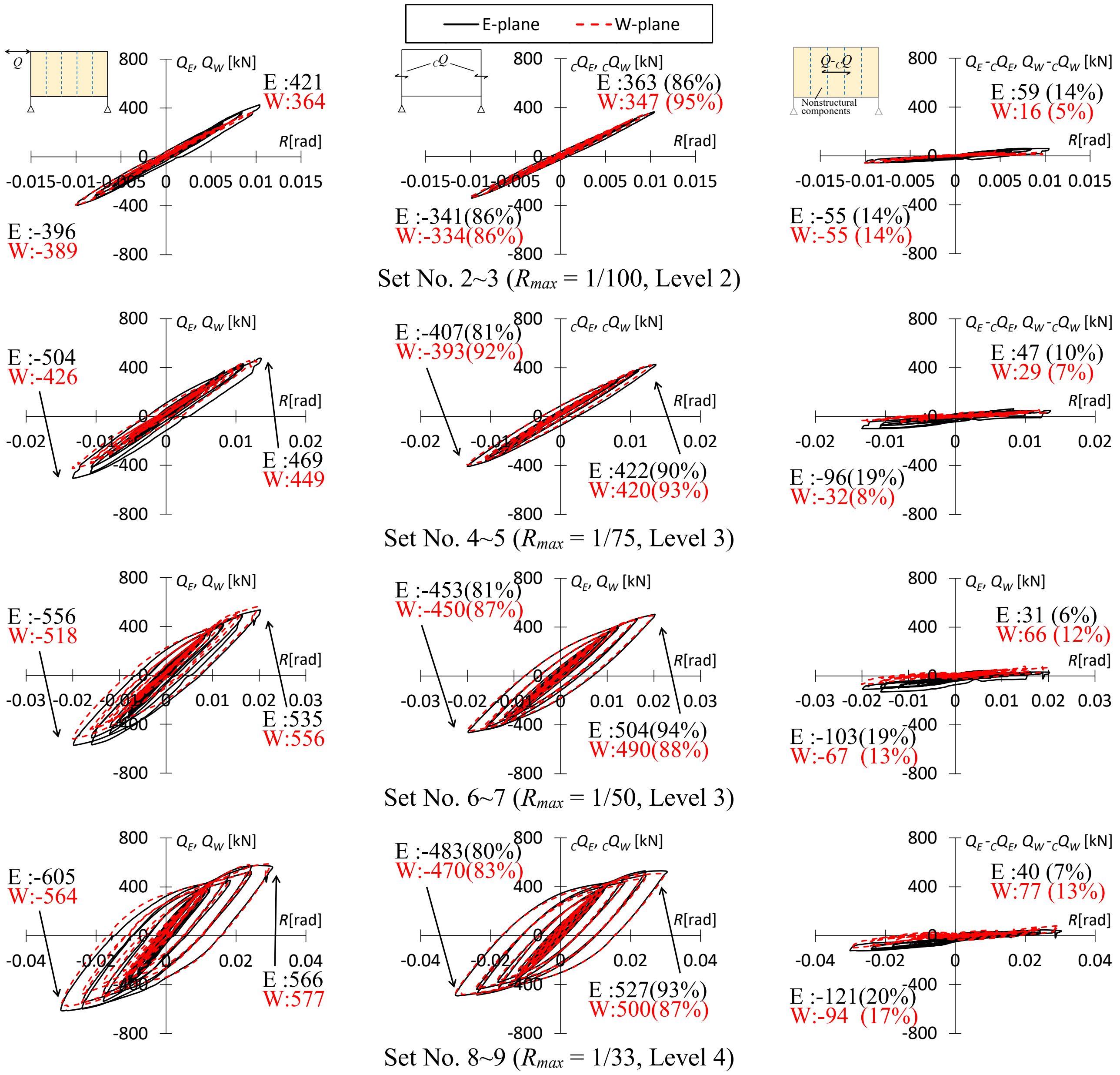

(a) Whole (b) Steel frame (c) Nonstructural components

Fig. 3 – Load-deformation relationship of ALC frame

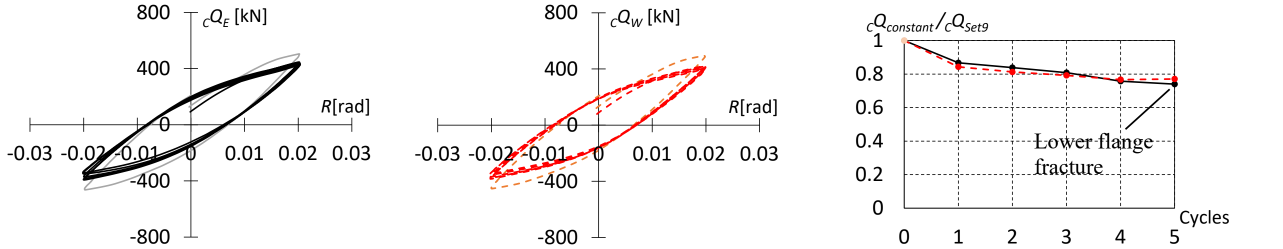

(a) E-plane (b) W-plane (c) Deterioration of maximum strength

Fig. 4 – Load-deformation relationship of the steel frame in constant amplitude loading (1/50) of ALC frame

From the load-deformation relationship of the steel frame ((b) in the figure), it could be seen that the strength of the steel frame in both specimens is almost the same. However, in terms of the strength of the whole specimen ((a) in the figure), the maximum strength is varied depending on the type (LGS or ALC) and the configuration (with/without opening and eccentric part) of the nonstructural component. Since the LGS wall is attached inside the steel frame, the LGS wall and the structure came into contact when the structure was deformed. As a result, a considerably large amount of shear force acts on the LGS wall. On the other hand, since the ALC wall was attached outside of the steel frame, the contact between the ALC wall and the structure did not occur even when the structure deformed. The shear force was only generated by the friction or contact caused by rocking between ALC panel which is relatively small compared to the direct contact in case of LGS frame. The percentage of shear force resisted by the nonstructural component are shown in the load-deformation relationship of the nonstructural component. On average, the shear force acting on the LGS wall is around 33% and 20% for E- and W-plane, respectively. On the other hand, the shear force resisted by the ALC wall on average is 17% and 8% for E- and W-plane, respectively. It also can be seen that the plane with openings and eccentric part resisted a lower amount of shear force compared to that of without any openings.

The load-deformation relationship of the steel frame in E-plane and W-plane are shown in Fig. 2(a-b) and 4(a-b). Meanwhile, the deterioration of maximum strength in the negative side is shown in Fig. 2(c) and 4(c). The vertical axis shown in (c) of the figures was the ratio of the maximum strength at each cycle in constant amplitude loading to the maximum strength at the same R in loading sets considering multiple earthquakes (1/33 (Set No. 9) for LGS frame and 1/50 (Set No. 7) for ALC frame). In the ALC frame, the maximum strength was similarly reduced due to local buckling at the beam end on both planes until the lower flange of the beam in E-plane was fully fractured (fifth cycle). Meanwhile, in the LGS frame, the strength of the E-plane was significantly reduced due to the fracture of the lower flange at the early cycle. In addition, it can be seen that in both planes both specimens, from the second cycle, the decrement of the maximum strength became smaller and smaller because the local buckling at the beam end hardly progressed.

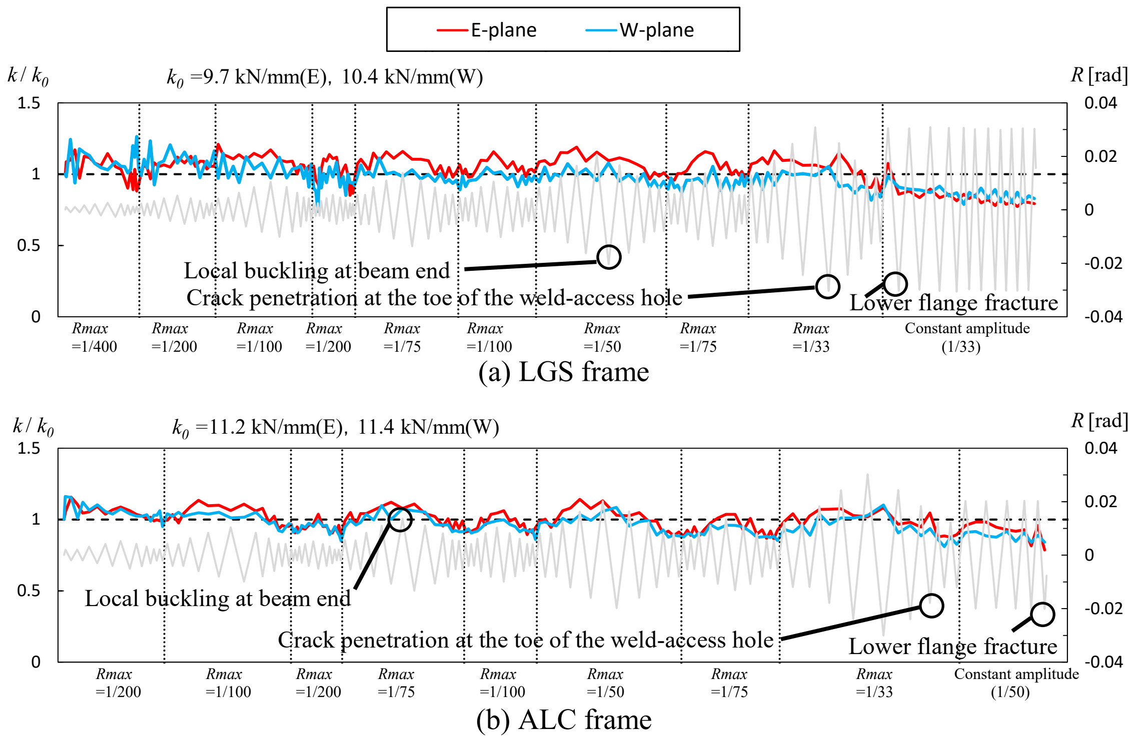

Fig. 5 – Transition of unloading stiffness

Fig. 5 shows the transition of the unloading stiffness (elastic stiffness) of the steel frame at each peak of the cycles for both specimens. The unloading stiffness was calculated from the time when the unloading was started to the point where the load decreased to 70% of the maximum strength of the corresponding cycle. The vertical axis of the graph is the value obtained by dividing the unloading stiffness by the initial elastic stiffness. The initial elastic stiffness was calculated from the point at which loading was started to the point where the load reaching 30% of the maximum strength of the first cycle for each frame. In both specimens, the stiffness hardly decreased even after the local buckling of the beam occurred in Set No. 5 or 7 (Level 3). The stiffness was slightly reduced due to the progress of the local buckling at the beam end in Set No. 9 (Level 4) and greatly reduced after the first cycle of constant amplitude loading because the lower flange of the lower beam in E-plane of LGS frame was fractured.

4. Conclusions

In this study, a cyclic loading test of SMRF was conducted. Two specimens were tested considering the variations in the beam-to-column connection detail, i.e., with and without the weld access hole, and the type of the nonstructural component, i.e., LGS wall and ALC wall. To simulate the multiple earthquakes, one typical loading set that corresponds to one earthquake was created using the time history response analysis result. During the test, the maximum story drift angle (R_{max}) of the typical loading set was adjusted to various levels of an earthquake, and multiple loading set with various levels was performed to simulate the occurrence of multiple earthquakes. The obtained findings from the experiment are summarized below.

- Comparing the damage generated within the structural and nonstructural components, the damage of the LGS wall was found when there was almost no damage in the ALC wall and steel frame. Therefore, it could be concluded that the functionality continuity of buildings excited by multiple earthquakes might be determined by the damage of the LGS wall rather than the steel frame or the ALC wall.
- There was almost no deterioration in stiffness at the story level after the steel frames experienced loading sets of R_{max} [1/200 × 2] + [1/100 × 2] + [1/75 × 2] + [1/50 × 1] even though a small crack at the toe of weld access hole and a small deformation of local buckling at the beam ends were observed. Both steel frame specimens show deterioration in stiffness after subjected to a loading set of R_{max} 1/33 because the local buckling of the beam progressed even more.
- On both specimen, at the end of the loading, the lower flange of the beam in steel frames with weld access hole connection detail was completely fractured, while in that of without weld access hole connection detail, only a slight crack was generated at the weld toe. In addition, the strength and stiffness deteriorated more in the steel frame with weld access hole connection detail because the lower flange section was completely fractured. Those comparisons show that the connection detail without the weld access hole performs better under the excitation of multiple earthquakes.
- The shear force resisted by the nonstructural components is found to be depending on the type and the configuration of nonstructural components. On average, the ratios of shear force resisted by the LGS wall with and without openings and eccentric parts are about 20% and 33%, respectively; and for the ALC with and without openings, the ratios are about 8% and 17%, respectively. Thus, the influence of nonstructural components is particularly significant when all the LGS wall is attached in-plane without any openings.

Acknowledgement

This work is supported by Japan Society for the Promotion of Science KAKENHI Grant Number JP17H01302. Deck plates were provided by Composite Slab Industrial Association, and driving pins were provided by Max Co. Ltd. Their financial supports are gratefully acknowledged. The authors also thank Dr. Norihito Miki for his support during the preparation of the experiment.

